

This work was written as part of one of the author's official duties as an Employee of the United States Government and is therefore a work of the United States Government. In accordance with 17 U.S.C. 105, no copyright protection is available for such works under U.S. Law.

Public Domain Mark 1.0

<https://creativecommons.org/publicdomain/mark/1.0/>

Access to this work was provided by the University of Maryland, Baltimore County (UMBC) ScholarWorks@UMBC digital repository on the Maryland Shared Open Access (MD-SOAR) platform.

Please provide feedback

Please support the ScholarWorks@UMBC repository by emailing scholarworks-group@umbc.edu and telling us what having access to this work means to you and why it's important to you. Thank you.

Wave-Vector Dependence of Magnetic-Turbulence Spectra in the Solar Wind

Y. Narita* and K.-H. Glassmeier†

*Institut für Geophysik und extraterrestrische Physik, Technische Universität Braunschweig,
Mendelssohnstraße 3, D-38106 Braunschweig, Germany*

F. Sahraoui‡ and M. L. Goldstein

Geospace Physics Laboratory, NASA Goddard Space Flight Center, Code 673, Greenbelt, Maryland 20771, USA

(Received 31 January 2008; published 28 April 2010)

Using four-point measurements of the Cluster spacecraft, the energy distribution was determined for magnetic field fluctuations in the solar wind directly in the three-dimensional wave-vector domain in the range $|k| \leq 1.5 \times 10^{-3}$ rad/km. The energy distribution exhibits anisotropic features characterized by a prominently extended structure perpendicular to the mean field preferring the ecliptic north direction and also by a moderately extended structure parallel to the mean field. From the three-dimensional energy distribution wave vector anisotropy is estimated with respect to directions parallel and perpendicular to the mean magnetic field, and the result suggests the dominance of quasi-two-dimensional turbulence toward smaller spatial scales.

DOI: 10.1103/PhysRevLett.104.171101

PACS numbers: 96.50.Ci, 52.35.Ra

Magnetic field fluctuations in the solar wind often exhibit turbulence properties, as the fluctuations appear irregular and their frequency spectra can be approximated by a power law with the spectral index close to $-5/3$ [1–5], reminiscent of the inertial-range spectrum of hydrodynamic turbulence [6]. Of course, the solar wind represents a plasma flow and its turbulence behavior is different from ordinary fluid turbulence in many aspects: It is electrically conducting and allows the ambient magnetic field to fluctuate; fundamental motions unique to plasmas such as Alfvénic fluctuations may also be the carrier of energy cascade other than eddy distortions of fluid origin; small-scale fluctuations form a second inertial range at higher frequencies in the spectrum, transmitting energy from large scales to the smallest dissipation-range scales at about the electron gyro-radius or inertial length [7].

Here we study anisotropy of magnetic field fluctuations in the solar wind. Anisotropy in solar wind turbulence has been suggested in various studies. Earlier observations showed that correlation of magnetic field fluctuations tends to peak in the parallel and perpendicular directions to the mean magnetic field, and not in oblique directions [8]. The solar wind fluctuations are therefore often interpreted as a competition between two different fluctuation geometries: One is associated with parallel wave vectors to the mean magnetic field (referred to as the slab geometry) and the other is associated with perpendicular wave vectors (the two-dimensional turbulence geometry). Study of cosmic ray transport suggests that the two-dimensional turbulence geometry must play a dominant role to account for long mean free paths of cosmic rays [9,10]. On the other hand, an extensive correlation analysis suggests that the dominance of the two fluctuation geometries is case dependent: the slab geometry dominates in the fast streams and the

two-dimensional turbulence geometry in the slow streams [11]. Previous attempts at direct measurement of the symmetry properties of solar wind turbulence are based on single spacecraft data and the analyses were limited to one or two dimensions using Taylor's hypothesis [12] and the assumption of axisymmetric fluctuations around the mean magnetic field.

With the advent of the Cluster mission [13] it has become possible to determine energy distributions directly in the three-dimensional wave-vector domain, which provides more complete information about the fluctuation properties. Cluster consists of four identical spacecraft, flying in tetrahedral formation in near-Earth space. Using multispacecraft data, correlation studies of solar wind turbulence were presented in various papers [14–17]. Here we measure the magnetic energy distribution in the three-dimensional wave-vector domain using Cluster data and the wave telescope technique, and compare the fluctuation energy associated with the two distinct wave-vector geometries. The analysis does not make use of Taylor's hypothesis.

The upper panels in Fig. 1 display time series data of the magnetic field strength, the flow speed, and the ion number density in the solar wind measured by the fluxgate magnetometer [18] and the electrostatic ion analyzer [19] on board Cluster-1 for a 4-h interval on March 12, 2005, 1800–2200 UT. The solar wind is in a slow stream interval with the mean flow speed 364 km/s and the mean density 3.6 cm^{-3} . The mean magnetic field strength is 1.9 nT. This interval represents one of the relatively stationary solar wind intervals with some foreshock signatures measured by Cluster while in an almost regular tetrahedral configuration. Such a near-perfect tetrahedral configuration is necessary to minimize spatial aliasing effects [20]. The

spacecraft are located near the orbit apogee ($19R_E$, where $1R_E = 6371$ km) ahead of the Earth with the mean spacecraft separation about 1000 km. The magnetic field fluctuations exhibit a power-law spectrum in the frequency domain (in the spacecraft frame) with the spectral index close to $-5/3$, which is often observed by many spacecraft (Fig. 1 lower panel).

We take a parametric approach for power spectrum estimation with the following steps. First, we determine a 12×12 cross spectral density (CSD) matrix in the frequency domain. Here the 12 components represent 3 components of the magnetic field measured by 4 spacecraft. The time interval is split into 100 windows with the length 256 s and the CSD matrix is determined for each time window and then averaged over the windows. Second, the CSD matrix is projected into a 3×3 matrix (representing 3 components of the magnetic field) in the four-dimensional frequency-wave-vector domain using the wave telescope technique (named also k filtering) [21–23]. In this projection method the filter coefficients are chosen so as to minimize the variance of the filter output, subject to the two constraints that the response of the filter is equal to unity at the looking wave vector (which is our parameter) and that the field is divergence free. The filter coefficients are determined not only by the wave vector but also by the measured CSD matrix itself. Previous studies using this technique have revealed turbulence properties in the Earth's foreshock region [24] and the Earth's magnetosheath region [25]. Third, we obtain the fluctuation energy

by taking the trace of the reduced matrix as a function of frequency and wave vector in the spacecraft frame. The energy distribution is then transformed into the plasma rest frame by correcting the Doppler shift. The mean flow velocity vector obtained by the electrostatic ion analyzer of Cluster is used in performing the Doppler correction. The distribution is determined in the wave number range up to 0.0015 rad/km and the rest frame frequency range up to 0.20 rad/s, close to the proton cyclotron frequency but still in the low-frequency regime. Finally, the distribution is integrated over the rest frame frequencies and the three-dimensional energy distribution is obtained. Details of the analysis method are discussed in [20,26].

Although the wave telescope is a projection method of the CSD matrix into arbitrary wave vectors, there are practical limits of wave vectors in the analysis. The upper limit (the highest wave number) is determined by the sensor separation distance due to the sampling theorem, while at lower wave numbers the estimated spectrum is gradually deformed due to an irregular tetrahedral configuration of spacecraft. Computer experiment of the wave telescope technique using synthetic data shows that the relative error of the wave vector remains small (less than 5%) down to wave numbers about 1/4 of the highest wave number: The relative error becomes larger than unity at very low wave numbers, smaller than 1/50 of the highest wave number [20]. In the following we present three- and two-dimensional spectra in a broad wave number range for qualitative inspection of anisotropy and then we limit one-dimensional spectra to a narrow wave number range in which the quantitative analysis is valid.

Figure 2 displays the three-dimensional energy distribution $E(\mathbf{k})$ in two different coordinate systems: the geocentric-solar-ecliptic (GSE) system and the mean-field-aligned (MFA) system. While the former uses the sunward and the ecliptic north directions as x and z axes, respectively, the latter uses the mean magnetic field and the maximum power direction in the plane perpendicular to the mean field as k_{\parallel} and $k_{\perp 1}$ components, respectively. The energy distributions are represented as projection onto three planes on a cube in the wave-vector domain (spanned by either k_x, k_y , and k_z or by $k_{\parallel}, k_{\perp 1}$, and $k_{\perp 2}$) by averaging over the wave-vector components perpendicular to the respective planes.

The 3D distribution is overall symmetric to changing the sign of the wave vector (reflection symmetry), but it is neither spherically nor axially. In the GSE coordinate system the primary extended structure appears in the ecliptic north direction (z axis, also almost perpendicular to the flow and the bow shock normal) and the secondary extended structure is in the y direction. In the analyzed time interval the mean magnetic field is almost aligned with the y direction, and therefore the primary and the secondary extended structures are associated with the directions perpendicular and the parallel to the mean magnetic field, too.

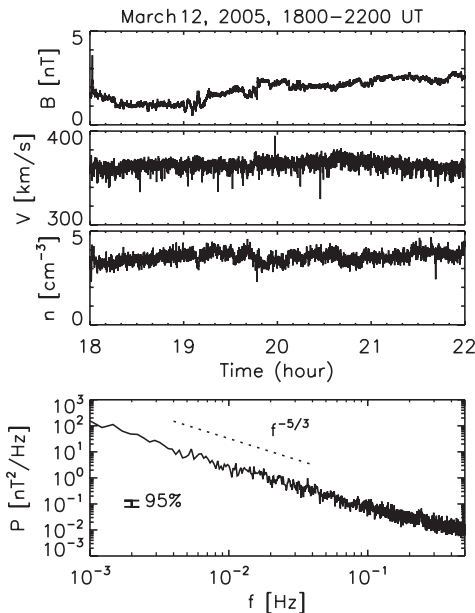


FIG. 1. Upper three panels display time series data of magnetic field strength, flow speed, and ion number density in the solar wind measured by Cluster-1 spacecraft. Lower panel displays power spectrum of the magnetic field fluctuation at the same spacecraft. Confidence interval is also plotted in the spectrum.

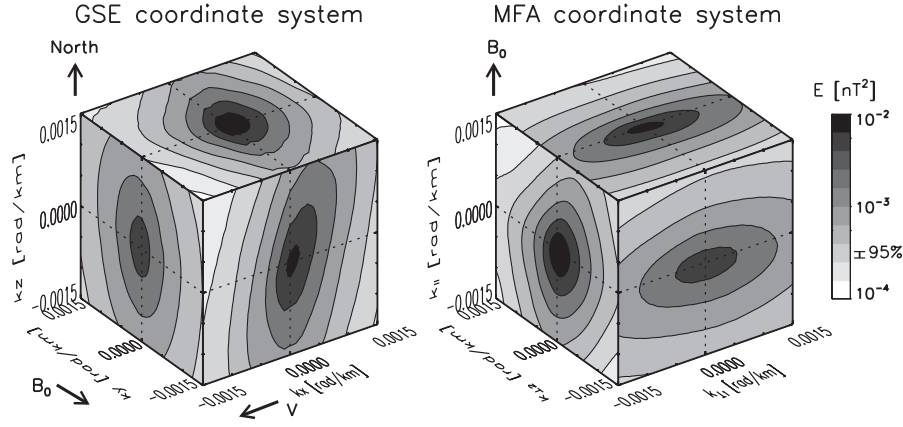


FIG. 2. Cubic representation of magnetic energy distribution in the three-dimensional wave-vector domain for the solar wind data shown in Fig. 1. The left-hand panel shows the distribution in the GSE coordinate system. The right-hand panel shows the distribution in the MFA system with k_{\parallel} , $k_{\perp 1}$, and $k_{\perp 2}$ components relative to the mean magnetic field \mathbf{B}_0 . The $k_{\perp 1}$ and the $k_{\perp 2}$ axes are in the maximum and minimum power directions in the perpendicular plane. In each coordinate system the three-dimensional data are projected onto three planes by averaging over the wave-vector components perpendicular to the planes. The 95% confidence interval is displayed at the contour scale bar. Directions of the mean magnetic field \mathbf{B}_0 , the ecliptic north, and the mean flow direction \mathbf{V} are indicated as well.

The association with the mean field can be seen more clearly in the MFA coordinate system. The primary extended structure appears in the $k_{\perp 1}$ - k_{\parallel} plane and the $k_{\perp 1}$ - $k_{\perp 2}$ plane. The distribution also shows that axisymmetry fails around the mean magnetic field. The secondary extended structure is almost in the parallel direction to the mean field ($k_{\perp 2}$ - k_{\parallel} plane). The small vertical line at the contour scale bar represents the 69% confidence interval of the determined energy. We use a χ^2 distribution with 1200 degrees of freedom (averaging over 100 time windows and 12 elements of the CSD matrix) [27]. The confidence interval is smaller than the contour scale and assures the small statistical error.

Anisotropy in the energy distribution is evaluated in the following fashion. The three-dimensional distribution in the MFA coordinate system is reduced to two-dimensional distributions in the $k_{\perp 1}$ - k_{\parallel} plane and in the $k_{\perp 2}$ - k_{\parallel} plane. Since the distribution is not axisymmetric around the mean magnetic field, we retain the two perpendicular wave-vector components. The distributions are then summed over the sign of the wave vector. Figure 3 displays the two distributions in which the wave-vector components are given in absolute values. The distribution in the $k_{\perp 1}$ - k_{\parallel} plane exhibits the primary extended structure perpendicular to the mean field, while that in the $k_{\perp 2}$ - k_{\parallel} plane exhibits the secondary extended structure parallel to the mean field.

The two-dimensional distributions are further reduced to one-dimensional distributions and then transformed into the energy spectra as functions of k_{\parallel} , $k_{\perp 1}$, and $k_{\perp 2}$, respectively, by dividing the 1D energy distributions by the intervals of the wave-vector components. Figure 4 upper panel displays the three energy spectra in the wave number range $5.0 \times 10^{-4} \leq k \leq 1.5 \times 10^{-3}$ rad/km. Beyond this range the determined energy has larger uncertainties due to

(1) spatial aliasing, (2) asymmetric coverage of the wave-vector domain due to the flow effect (limiting the highest wave number), and (3) distortion effect induced by the measurement (limiting the lowest wave number) [20,26]. The $E(k_{\perp 1})$ spectrum contributes most to the fluctuation energy; $E(k_{\parallel})$ has the second contribution and $E(k_{\perp 2})$ the smallest. The power law with the index $-5/3$ is also shown in the figure for comparison. The spectrum $E(k_{\perp 1})$ is well fitted by this power law, although one should not immediately conclude that this energy spectrum is representative

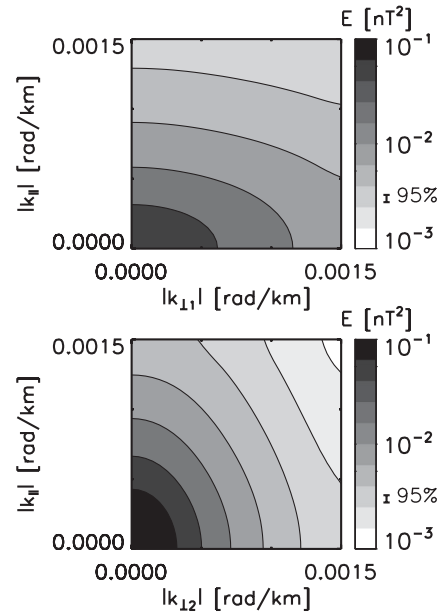


FIG. 3. Two-dimensional energy distributions in the MFA system. The distributions are folded (summed) over the sign of the wave vector.

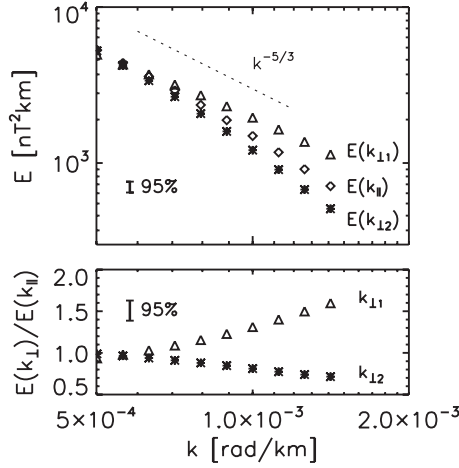


FIG. 4. One-dimensional energy spectra for the three wave-vector components (upper panel) and the ratios $E(k_{\perp 1})/E(k_{\parallel})$ and $E(k_{\perp 2})/E(k_{\parallel})$ compared at the same wave numbers (lower panel). The error bars represent the statistical error shown in Fig. 2.

for solar wind turbulence since our measurement is limited to the wave number range less than 1 order of magnitude. The energy spectra for the two perpendicular wave-vector components are compared to that for the parallel wave-vector component (Fig. 4 lower panel). The ratio $E(k_{\perp 1})$ to $E(k_{\parallel})$ increases from almost unity at the lowest wave number to about 1.6 at the highest wave number, reflecting the primary extended structure. On the other hand, the ratio $E(k_{\perp 2})$ to $E(k_{\parallel})$ decreases from almost unity to about 0.7, and this reflects the secondary extended structure parallel to the mean field.

Determining energy distributions with Cluster data opens the gate for studying solar wind turbulence in the full three-dimensional space. Although the analysis is limited to a small range in the wave-vector domain, our measurement provides (1) the direct evidence of the dominance of the perpendicular wave-vector geometry or quasi-two-dimensional turbulence in solar wind supporting the previous results based on single spacecraft data [8,11,14] as well as (2) the lack of axisymmetry which was not seen before the Cluster mission. We obtain the energy anisotropy ratio of the perpendicular to the parallel wave-vector geometry about 1.6 at the higher wave number, which is smaller than the ratio about 4 derived from the study of cosmic ray transport [9]. Recent studies based on single spacecraft method of Cluster data show that magnetic field fluctuations on kinetic scales smaller than ion gyroradius or ion inertial length are associated with highly oblique wave vectors from the mean magnetic field direction [7]. It is therefore an interesting question how anisotropy develops from larger scales of the order of 10 000 km to smaller scales of the order of 100 km using Cluster data.

This work is financially supported by Bundesministerium für Wirtschaft und Technologie and Deutsches Zentrum für Luft- und Raumfahrt under Contract No. 50 OC 0901. We thank H. Rème and I. Dandouras for providing ion data of Cluster.

*y.narita@tu-bs.de

†Also at: Max-Planck-Institut für Sonnensystemforschung, Max-Planck-Straße 2, D-37191 Katlenburg-Lindau, Germany.

‡Now at: Laboratoire de Physique des Plasmas, CNRS-Ecole Polytechnique, Vélizy, 78140, France.

- [1] P. J. Coleman, *Astrophys. J.* **153**, 371 (1968).
- [2] W. H. Matthaeus and M. L. Goldstein, *J. Geophys. Res.* **87**, 6011 (1982).
- [3] W. H. Matthaeus, M. L. Goldstein, and C. W. Smith, *Phys. Rev. Lett.* **48**, 1256 (1982).
- [4] E. Marsch and C.-Y. Tu, *J. Geophys. Res.* **95**, 8211 (1990).
- [5] J. J. Podesta, D. A. Roberts, and M. L. Goldstein, *Astrophys. J.* **664**, 543 (2007).
- [6] A. N. Kolmogorov, *Dokl. Akad. Nauk SSSR* **30**, 299 (1941).
- [7] F. Sahraoui *et al.*, *Phys. Rev. Lett.* **102**, 231102 (2009).
- [8] W. H. Matthaeus, M. L. Goldstein, and D. A. Roberts, *J. Geophys. Res.* **95**, 20673 (1990).
- [9] J. W. Bieber *et al.*, *Astrophys. J.* **420**, 294 (1994).
- [10] J. W. Bieber, W. Wanner, and W. H. Matthaeus, *J. Geophys. Res.* **101**, 2511 (1996).
- [11] S. Dasso, L. J. Milano, W. H. Matthaeus, and C. W. Smith, *Astrophys. J.* **635**, L181 (2005).
- [12] G. I. Taylor, *Proc. R. Soc. A* **164**, 476 (1938).
- [13] C. P. Escoubet, M. Fehringer, and M. Goldstein, *Ann. Geophys.* **19**, 1197 (2001).
- [14] T. Osman and T. Horbury, *Astrophys. J.* **654**, L103 (2007).
- [15] T. Osman and T. Horbury, *J. Geophys. Res.* **114**, A06103 (2009).
- [16] S. Dasso *et al.*, in *Proceedings of the 30th International Cosmic Ray Conference, Merida, Mexico, 2007* (Universidad Nacional Autonoma de Mexico, Mexico City, 2008), Vol. 1, p. 625.
- [17] Weygand *et al.*, *J. Geophys. Res.* **114**, A07213 (2009).
- [18] A. Balogh *et al.*, *Ann. Geophys.* **19**, 1207 (2001).
- [19] H. Rème *et al.*, *Ann. Geophys.* **19**, 1303 (2001).
- [20] F. Sahraoui, G. Belmont, M. L. Goldstein, and L. Rezeau, *J. Geophys. Res.* **115**, A04206 (2010).
- [21] J. L. Pinçon and F. Lefeuvre, *J. Geophys. Res.* **96**, 1789 (1991).
- [22] U. Motschmann *et al.*, *J. Geophys. Res.* **101**, 4961 (1996).
- [23] K.-H. Glassmeier *et al.*, *Ann. Geophys.* **19**, 1439 (2001).
- [24] Y. Narita, K.-H. Glassmeier, and R. A. Treumann, *Phys. Rev. Lett.* **97**, 191101 (2006).
- [25] F. Sahraoui *et al.*, *Phys. Rev. Lett.* **96**, 075002 (2006).
- [26] Y. Narita, F. Sahraoui, M. L. Goldstein, and K.-H. Glassmeier, *J. Geophys. Res.* **115**, A04101 (2010).
- [27] G. M. Jenkins and D. G. Watts, *Spectral Analysis and its Applications* (Holden-Day, San Francisco, 1968), p. 313.